Experimental Neurology 401 (2026) 115758

Contents lists available at ScienceDirect

Experimental Neurology

journal homepage: www.elsevier.com/locate/yexnr

Research paper

# Revealing subcellular retinal alterations in 5xFAD B6SJLF1/J mice

A. Giani [a,b,1], C.A. Musi [a,b,1], E.C. Priori [a,b], S. Turchetti [c,b], M. Passi [a,b], S. Galbiati [d], I. Viganò [d], N. Bakker [e], I. Klaassen [e], G. Zerbini [d], T. Borsello [a,b,*], on behalf of the RECOGNISED consortium

[a] Department of Pharmacological and Biomolecular Sciences, University of Milan, Milan, Italy
[b] Department of Neuroscience, IRCCS-Mario Negri Institute for Pharmacological Research, Milan, Italy
[c] Department of Life and Environmental Sciences, Marche Polytechnic University, Ancona, Italy
[d] Complications of Diabetes Unit, Diabetes Research Institute, IRCCS Ospedale San Raffaele, Milan, Italy
[e] Ocular Angiogenesis Group, Department of Ophthalmology, Amsterdam UMC location University of Amsterdam, Amsterdam, the Netherlands

ARTICLE INFO

*Keywords:*
Alzheimer diseases
Neurodegeneration
JNK3
PSD95 phosphorylation
Gliosis
Amyloid pre-cursor protein
Retinal thickness

ABSTRACT

The 5xFAD mouse model recapitulates key pathological features of Alzheimer's disease (AD). However, it remains unclear whether JNK activation represents a common pathogenic mechanism driving both retinal and cerebral neurodegeneration. Establishing such a shared pathway would significantly enhance the retina's potential as an accessible window into the central nervous system (CNS) for monitoring AD progression.

We analyzed total retinal homogenates and postsynaptic-enriched protein fractions from 2, 4, 6, and 10-month-old 5xFAD B6SJLF1/J mice using Western blotting and immunofluorescence staining. Key markers of JNK signaling (JNK, p-JNK, JNK3, c-Jun, p-c-Jun) and synaptic integrity (PSD95, p-PSD95) were examined. Additionally, we assessed gliosis (GFAP) and amyloid pathology (APP, p-APP) to evaluate retinal AD progression. Finally, we compared retinal layer thickness between 5xFAD and wild-type (WT) mice across these age points.

Although Western blotting revealed no significant JNK signaling activation in total retinal homogenates, synaptic dysfunction was evident through increased PSD95 phosphorylation in 5xFAD mice. Immunofluorescence analysis demonstrated elevated JNK3 immunoreactivity and gliosis in transgenic animals compared to controls. Notably, while WT mice exhibited age-related inner nuclear layer (INL) thinning, 5xFAD mice maintained stable INL thickness and showed progressive total retinal thickening.

These findings demonstrate fundamental differences in AD pathology between retinal and brain tissues in 5xFAD B6SJLF1/J mice. The weak JNK activation signature observed in retinal tissue, contrasting with robust brain pathology, suggests current limitations in developing retinal biomarkers for AD detection. Furthermore, our results underscore the necessity of both technical refinement and cautious cross-species interpretation when evaluating the retina's potential as a CNS disease monitor.

## 1. Introduction

Alzheimer's disease (AD) is a progressive neurodegenerative disorder characterized by a gradual and irreversible decline in cognitive and functional abilities. Current treatments are primarily symptomatic and aim to slow the progression of the disease rather than provide a definitive solution (Safiri et al., 2024). Recently, two anti-amyloid therapies have been approved for early-stage Alzheimer's disease, marking a milestone in disease-modifying treatment. Lecanemab (Leqembi) received FDA approval in January 2023, and donanemab (Kisunla) was approved in July 2024. Both are monoclonal antibodies targeting amyloid plaques, aimed at reducing amyloid burden and slowing cognitive decline in patients with early symptomatic AD.

The pathological features of AD include the accumulation in the brain of amyloid β (Aβ) plaques and the formation of neurofibrillary tangles (NFTs) of hyperphosphorylated tau (pTau). These pathological processes drive synaptic dysfunction and neuronal degeneration, ultimately leading to cognitive impairment.

* Corresponding author at: Neuronal Death and Neuroprotection Lab, Department of Pharmacological and Biomolecular Sciences, Università degli Studi di Milano, Via Balzaretti 9, 20133 Milan, Italy.
*E-mail address:* tiziana.borsello@unimi.it (T. Borsello).
[1] These authors contributed equally to this work.

https://doi.org/10.1016/j.expneurol.2026.115758
Received 11 September 2025; Received in revised form 7 March 2026; Accepted 31 March 2026
Available online 1 April 2026

The absence of a resolutive cure for AD is primarily due to its multifactorial pathology and the brain's limited accessibility, which makes it difficult to identify the onset and progression of degenerative processes.

Recent evidence suggests that the retina may serve as a window into brain parenchyma. As an extension of the central nervous system (CNS), the retina shares an embryonic origin with the brain and exhibits similar responses to neuronal damage. This connection is reinforced by clinical observations in type 2 diabetes (T2D), where diabetic retinopathy frequently coexists with cognitive impairment and dementia (Biessels et al., 2006; Kopf and Frölich, 2009).

Retinal neural degeneration in AD was first reported in 1986 (Hinton et al., 1986); showing ganglion cell loss and optic nerve fiber degeneration in post-mortem AD retinas. Optical coherence tomography (OCT); now the gold standard for retinal imaging; has since revealed AD-related retinal changes; including thinning of the peripapillary retinal nerve fiber layer (pRNFL); ganglion cell-inner plexiform layer (GC-IPL); macula volume; and choroid (Doustar et al., 2017; Gaire et al., 2024; Jin et al., 2025). Similar thinning has been seen in mild cognitive impairment (MCI) patients, correlating with AD severity and cognitive decline (Parisi et al., 2001). Aβ plaques have also been detected in AD retinas (Gaire et al., 2024). However; collecting longitudinal data on elderly populations can be challenging. Consequently; transgenic mice serve as a valuable model for studying AD-related changes in the CNS and retina and for assessing drug efficacy (Olivares Ordoñez et al., 2025).

Retinal accumulation of Aβ has been observed in multiple transgenic mouse models of AD, though the timing of plaque formation varies across models (Alexandrov et al., 2011; Dutescu et al., 2009). For instance, 5xFAD mice, with a C57BL/6J pure background, exhibit the earliest plaque formation at 2 months, while Tg2576 mice exhibit the latest at 10 months (Lim et al., 2020; Salobrar-Garcia et al., 2020; Vandenabeele et al., 2021). Notably, in APPSWE/PS1△E9 mice, retinal Aβ plaques appear earlier than brain plaques, suggesting retinal changes precede brain pathology (Bevan et al., 2020; Chiquita et al., 2019).

Functional retinal degeneration, including RNFL thinning and ganglion cell activity shifts, begins early and progresses with disease severity. Retinal thinning correlates with broader neurodegenerative changes, making the retina a potential early marker for AD progression.

Although evidence is growing, the link between retinal, brain abnormalities and cognitive impairment remains unclear. Identifying shared pathogenic mechanisms and therapeutic targets between the brain and retina is crucial for identifying measurable retinal indicators for brain damage, paving the way for new diagnostic and therapeutic advancements.

c-Jun N-terminal kinase (JNK) plays a critical role in Alzheimer's disease and retinal degeneration. The JNK family consists of three main isoforms, JNK1, JNK2, and the neuron-enriched JNK3, which typically appear at ~46 kDa and ~ 54 kDa, and collectively regulate stress-responsive signaling pathways highly relevant to neurodegeneration. In AD, JNK contributes to Aβ plaque formation and tau tangle pathology by phosphorylating of APP and tau. Additionally, it disrupts synaptic function through glutamate receptors mislocalisation. In the retina, JNK activation is involved in retinal ganglion cell loss, vascular endothelial growth factor (VEGF) expression, and photoreceptor death (Du et al., 2013; Galy et al., 2005; Guma et al., 2009; Kang et al., 2012; Ploia et al., 2011; A. Sclip et al., 2014; Alessandra Sclip et al., 2011, 2013). In the context of AD; the CRND8 AD model showed increased JNK and c-Jun activation in both the retina and the brain (Buccarello et al., 2017). This suggests that JNK activation in both areas is linked to Aβ oligomer production and neuronal degeneration; making JNK a common player in the retina and brain. In the 5xFAD mouse model on B6SJLF1/J hybrid background; amyloid plaque deposition in the brain begins at 2 months; during the presymptomatic phase; while cognitive decline becomes apparent by 3.5 months (Priori et al., 2023). In this model, JNK activation also correlates with post-synaptic density alterations and early-stage memory impairment, underscoring its pivotal role in AD pathogenesis.

Using Western blotting and immunofluorescence, we examined whether neurodegeneration occurs earlier in the retina in this model and whether JNK activation represents a shared pathogenic pathway in retinal and brain degeneration. We longitudinally analyzed mice using OCT to assess retinal alterations focusing on four different time points to mirror the progression of AD: 2 months of age (pre-symptomatic phase), 4 months of age (prodromic phase), 6 months of age (advanced phase), and 10 months of age (late-stage disease).

## 2. Materials and methods

### 2.1. Mice

5xFAD mice (B6SJL-Tg (APPSwFlLon, PSEN1*M146L*L286V) 6799Vas/Mmjax Strain #034840-JAX) on a B6SJLF1/J background were obtained from the Jackson Laboratory. Age-matched wild-type (WT) littermates were used as controls. Hemizygous male mice (not carriers for the Pde6brd1 gene) were bred to B6SJLF1/J female mice (carriers for the Pde6brd1 gene) at the Mario Negri Institute for Pharmacological Research IRCCS animal facility (Priori et al., 2023). Procedures involving animals and their care were conducted by national and international laws and policies (Permit Number 4/2021-PR). The experimental design included two groups: Tg-5xFAD B6SJLF1/J mice and WT mice. Blind (homozygous for mutation in the Pde6brd1 gene) and heterozygous mice were not included in the experiment. Both male and female Tg-5xFAD B6SJLF1/J and WT mice were assessed at four ages: 2 months ($n = 7$ per group), 4 months (n = 7 per group), 6 months (n = 7 per group) and 10 months (n = 7 per group). Specifically, for each group (WT and TG), four males and three females were included at each time point. Animals were sacrificed by decapitation and retinas were extracted from the eyes of Tg-5xFAD B6SJLF1/J and WT. Retinal tissues were stored at −80 °C until further processing.

### 2.2. Genotyping

Genotyping was conducted using PCR, using a standard protocol provided by the Jackson Laboratory, using the GoTaq®G2 Flexi DNA polymerase kit (Promega, Madison, WI, USA). Tg-5xFAD B6SJLF1/J and WT mice were tested for APP and Pde6brd1 genes.

### 2.3. Triton X-100 insoluble fractionation (TIF)

Animals were sacrificed and the retina was extracted to perform biochemical analysis. Subcellular fractionation was performed as reported in the literature (Gardoni et al., 2001a; Gardoni et al., 2012; Musi et al., 2020), with minor modifications. Briefly, the tissue was homogenized with a glass-glass Potter apparatus in 0.32 M ice-cold sucrose (S0389) buffer containing the following concentrations: 1 mM HEPES (H3375), 1 mM $MgCl_2$ (M8266), 1 mM $NaHCO_3$ (S5761), 10 mM NaF (71519) and 0.1 mM PMSF (P7626) at pH 7.4 (all from Sigma-Aldrich Darmstadt, Germany), with a complete set of protease inhibitors and phosphatase inhibitors (4,693,124,001, 04906837001, Roche Diagnostics, Basel, Switzerland). A portion of the sample was stored at −80 °C as total homogenate, while the remaining part was processed for TIF. Samples were centrifuged at 17,900 ×*g*, for 15 min at 4 °C and the supernatant was removed. The pellet was resuspended in a buffer containing 75 mM KCl (P5405), 1 mM HEPES, and 1% Triton X-100 (X100) (all from Sigma-Aldrich) plus protease and phosphatase inhibitors. The suspension was ultracentrifuged at 100,000 ×g for 1 h. After supernatant removal, the final pellet (TIF) was homogenized using a sonicator (SONOPLUS, Bandelin, Berlin, Germany) in 20 mM HEPES (H3375, Sigma-Aldrich) with a complete protease and phosphatase inhibitor cocktail. The homogenate was stored at −80 °C until further processing.

### 2.4. Western blot

Protein concentrations were quantified using the Bradford Assay (5,000,006, Bio-Rad Protein Assay, Hercules, CA, USA): 20 μg of total tissue homogenate and 10 μg of TIF extracted proteins were separated by 10% SDS polyacrylamide gel electrophoresis. PVDF membranes (1,620,177, Bio-Rad) were blocked in PBS-buffered saline with 5% non-fat milk powder (70,166, Sigma-Aldrich), and 0.1% Tween20 (P1379, Sigma-Aldrich) (1 h, RT). Primary antibodies were diluted in the same buffer and incubated overnight at 4 °C with the dilutions listed in Table 1. Blots were developed using horseradish-peroxidase-conjugated secondary antibodies (Santa Cruz Biotechnology, Dallas, TX, USA) and the ECL chemiluminescence system (Bio-Rad). Protein bands were quantified by densitometry using Quantity One software (Bio-Rad). Kinase activation was assessed by calculating the ratio of phosphorylated to total kinase levels, and values were expressed as fold change relative to WT animals. All experiments were performed with at least three independent replicates.

### 2.5. ELISA

The Mouse Aβ42 Elisa Kit (KMB3441, Invitrogen) was used to assess the presence of Amyloid beta 42 in the tissue homogenate of the retina of WT and Tg-5xFAD B6SJLF1/J mice according to the manufacturer's instructions. The calibration curve ranges between 3.12 and 200 pg/mL. In case of low values (below the limit of detection), the data were censored and substituted with a constant value, equal to half the limit of detection (1.56 pg/mL).

### 2.6. OCT

In vivo analysis of the retina was carried out as previously described (Zerbini et al., 2023). Briefly: optical coherence tomography of the retina was performed using Micron IV together with Image-Guided 830 nm OCT (Phoenix Research Laboratories, Pleasanton, CA, USA). After anesthesia with intraperitoneal injection of 80 mg/kg Ketamine, 10 mg/kg Xylazine (Sigma-Aldrich, Munich, Germany), mydriatic animals underwent OCT through a bidimensional scan (B-scan) of both eyes and results were finally averaged. Insight software (Phoenix Research Laboratories) was used to perform retinal layer segmentation and quantification.

**Table 1**
List of antibodies used in Western blots and IF analysis.

| Antigen | Host Species | Source | Dilution for WB | Dilution for IF |
|---|---|---|---|---|
| APP | Rabbit | PA1–4648, Invitrogen | 1:1000 | 1:50 |
| p-APP (Thr668) | Rabbit | 3823, Cell Signaling | 1:1000 | |
| p-APP (Thr668) | Rabbit | 6986, Cell Signaling | | 1:100 |
| p-JNK (Thr183/ Tyr185) | Rabbit | 9251, Cell Signaling | 1:1000 | 1:100 |
| JNK | Rabbit | 9252, Cell Signaling | 1:1000 | |
| JNK3 | Rabbit | 2305, Cell Signaling | 1:1000 | 1:200 |
| c-Jun | Rabbit | 9165, Cell Signaling | 1:1000 | |
| p-c-Jun (Ser73) | Rabbit | 06–659, Millipore | 1:1000 | |
| PSD95 | Mouse | 004CA10011435–25, Cayman | 1:4000 | |
| p-PSD95 (Ser295) | Rabbit | ab2930, Abcam | 1:4000 | |
| Actin | Mouse | MAB1501, Millipore | 1:5000 | |
| GFAP | Rabbit | Z0034, DAKO | | 1:500 |

### 2.7. RNA extraction, reverse transcription and droplet digital PCR

RNA was isolated from the retina of 3 WT and 3 Tg-5xFAD B6SJLF1/J mice (4 months old) using the Maxwell® RSC SimplyRNA Tissue Kit (Promega) following the manufacturer's instructions. The RNA was eluted in 50 μL of nuclease-free water and reverse transcribed using the High-Capacity cDNA Reverse Transcription Kit (Applied Biosystems, Waltham, Massachusetts, USA), generating cDNA at a final concentration of 25 ng/μl. Human and mouse APP expression levels were determined by droplet digital PCR (ddPCR) using a QX100 ddPCR platform (Bio-Rad). The final volume of the PCR mix was 20 μL, including 10 μL of ddPCR™ Supermix for Probes (No dUTP, Bio-Rad), 1 μL of probe (Human APP = dHsaCPE5046076 labelled in FAM, mouse APP = dMmuCPE5117707 labelled in HEX, Bio-Rad), and 2 μL (50 ng) of cDNA template. The droplet emulsion was thermally cycled using a C1000 Touch Thermal Cycler (Bio-Rad). Cycling conditions were 95 °C for 5 min, followed by 40 cycles of amplification (94 °C for 30 s and 55 °C for 1 min), and ending at 98 °C for 10 min, according to the manufacturer's protocol. The concentration of the target was calculated automatically using QuantaSoft™ software version 1.7.4 (Bio-Rad).

### 2.8. Immunofluorescence staining of mouse retina

For immunofluorescence staining of mouse retina, eyes of Tg-5xFAD B6SJLF1/J mice and WT mice were collected. Retinal cryostat sections (10 μm thick) were fixed in 4% (*w/v*) formaldehyde for 20 min and were washed once in 3× phosphate-buffered saline (PBS). For blocking, sections were incubated for 1 h or 30 min (only for APP) at room temperature (RT) with blocking solution composed of either 2% BSA, 0.1% Triton X-100 and 2% normal goat serum (NGS) in PBS (for APP); or 3% BSA, 0.5% Triton X-100 and 2% NGS in PBS (for p-APP); or 0.1% Triton X-100 and 10% NGS in PBS (for p-JNK and glial fibrillary acidic protein (GFAP)); or 0.5% Triton X-100 and 5% NGS in PBS (for JNK3). Directly after blocking, sections were incubated overnight at 4 °C with primary antibodies (Table 1). For negative controls, primary antibodies were omitted. Antibodies were diluted in blocking buffer (APP and p-JNK), in 1% BSA (p-APP) or in normal antibody diluent (AB999, Scytek) (for GFAP and JNK3). Sections were subsequently washed 3 times with PBS for 5 min and incubated with Isolectin GS-IB4 conjugated to Alexa Fluor™ 488 (I21411, Invitrogen; 1:50) and secondary antibodies goat anti-rabbit Alexa Fluor™ 633 (A21071, Invitrogen; 1:200) or goat anti-rabbit Cy3 (111–165-144, Jackson ImmunoResearch; 1:200). After washing 3 times with PBS for 5 min, sections were mounted with Vectashield antifade mounting medium with DAPI (H-1200–10, Vector Laboratories). Sections were imaged using a confocal laser scanning microscope (Leica, SP8) with settings kept constant between experimental groups. To quantify the global fluorescence for each retinal marker, we defined the region of interest (ROI) to include only the retinal layers in each image, excluding other ocular structures. The mean fluorescence intensity within this ROI was measured using ImageJ. For each eye, results were expressed as the mean value derived from all images. Statistical analyses were performed using GraphPad Prism v10 (GraphPad Software, La Jolla, USA). Student's *t*-test was used to compare WT and TG groups, with data presented as mean ± standard deviation.

### 2.9. Statistical analysis

Statistical analyses were performed with GraphPad Prism (version 10.2.0). For layer thickness measurements, individual eyes were included as independent samples. Data in Figs. 1–2 were analyzed using two-way ANOVA followed by Sidak's multiple-comparisons test. Data in Figs. 3–4d were analyzed using Welch's *t*-test. Data in Fig. 4c were analyzed using a mixed-effects analysis followed by Sidak's multiple-comparisons test. Data in Figs. 5 were analyzed using two-way ANOVA followed by Tukey's multiple-comparisons test. Data in Fig. 6

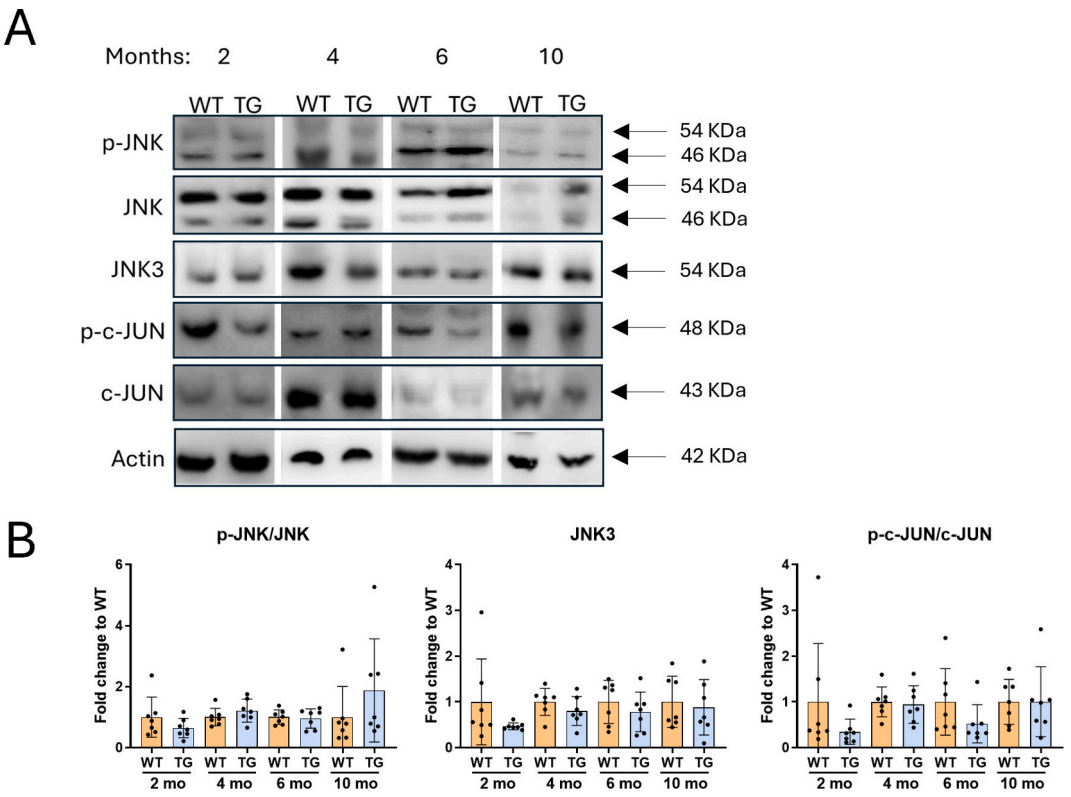


**Fig. 1.** JNK signaling pathway in retinal total homogenates of WT and 5xFAD B6SJLF1/J mice across different ages. A) Representative cropped images of Western blots of p-JNK, JNK, JNK3, p-c-Jun, c-Jun and β-actin (loading control) in retinal total homogenates from WT and 5xFAD B6SJLF1/J mice at 2, 4, 6, and 10 months of age. B) Quantification of protein levels relative to WT mice, presented as mean ± SD ($n = 7$ per time point).

were analyzed using the Kruskal–Wallis test followed by Dunn's multiple-comparisons test. A $P$ value $<0.05$ was considered statistically significant.

## 3. Results

### 3.1. The JNK signaling pathway is not active in retinal total homogenates of 5xFAD B6SJLF1/J mice

Previous work from our group demonstrated activation of the c-Jun N-terminal kinase (JNK) pathway in cortical total homogenates of 5xFAD B6SJLF1/J mice, with significant JNK activation detectable at 3.5 months of age, followed by induction of the c-Jun-mediated neuronal death pathway by 10 months(Priori et al., 2023). In the current study, we investigated whether this pathway is similarly activated in retinal total homogenates. Specifically, we assessed: (1) the ratio of phosphorylated JNK (p-JNK) to total JNK, (2) protein levels of JNK3 (the predominant CNS-specific JNK isoform), and (3) phosphorylated c-Jun to total c-Jun (the principal downstream effector of JNK signaling and a key transcriptional regulator of apoptotic cell death).

In contrast to our cortical findings, retinal analyses revealed no significant activation of JNK or c-Jun in 5xFAD B6SJLF1/J mice compared to WT controls at any examined time point (Fig. 1A, B). JNK3 expression levels also remained unchanged between genotypes and across all ages (Fig. 1A, B), further supporting the absence of JNK pathway engagement in the retina. This tissue-specific difference in JNK signaling dynamics points to intrinsic differences in stress vulnerability between cortical and retinal neurons in neurodegenerative disease.

### 3.2. Altered PSD95 levels in retinal neurons precede JNK activation during disease progression in 5xFAD B6SJLF1/J mice

We have previously demonstrated a disrupted organization of postsynaptic density (PSD) markers in the cortex of 5xFAD B6SJLF1/J mice (Priori et al., 2023). To determine whether similar alterations occur in the retina; we analyzed protein levels in the retinal postsynaptic-enriched protein fraction by isolating the Triton-insoluble fraction (TIF); which is known to represent the PSD region (Biggi et al., 2017; Gardoni et al., 2012; Gardoni et al., 2001b; Musi et al., 2020; Priori et al., 2023; A. Sclip et al., 2014; Alessandra Sclip et al., 2013).

We focused on on the postsynaptic compartment specifically the postsynaptic density fraction to examine molecular changes occurring directly at the synapse a critical hub for synaptic signaling and plasticity. Enriching for postsynaptic proteins enhances our ability to study PSD-95, a scaffold protein and direct target of JNK. This targeted approach increases sensitivity for detecting subtle, functionally relevant alterations that might otherwise be masked in analyses of total retinal protein, providing a more precise view of early synaptic dysfunction.

To assess whether JNK activation occurs selectively within the PSD region, we examined both: (1) JNK phosphorylation status in the TIF, and (2) JNK-mediated modulation of PSD95, a canonical JNK substrate and essential PSD scaffolding protein that organizes synaptic signaling complexes (Coffey, 2014; Musi et al., 2022; Zhou et al., 2023). While our previous work demonstrated early JNK pathway activation in cortical postsynaptic fractions (evidenced by increased p-JNK and p-PSD95 levels from 3.5 months of age), retinal analyses revealed distinct spatiotemporal patterns. At 4 months, we detected elevated p-PSD95 despite the absence of p-JNK (Fig. 2). Notably, retinal JNK activation only became apparent at 10 months. Together, these findings suggest a compartmentalized and delayed JNK-mediated stress response in the retina compared to cortical neurons, highlighting distinct spatiotemporal patterns of neurodegenerative pathology in the CNS of 5xFAD mice.

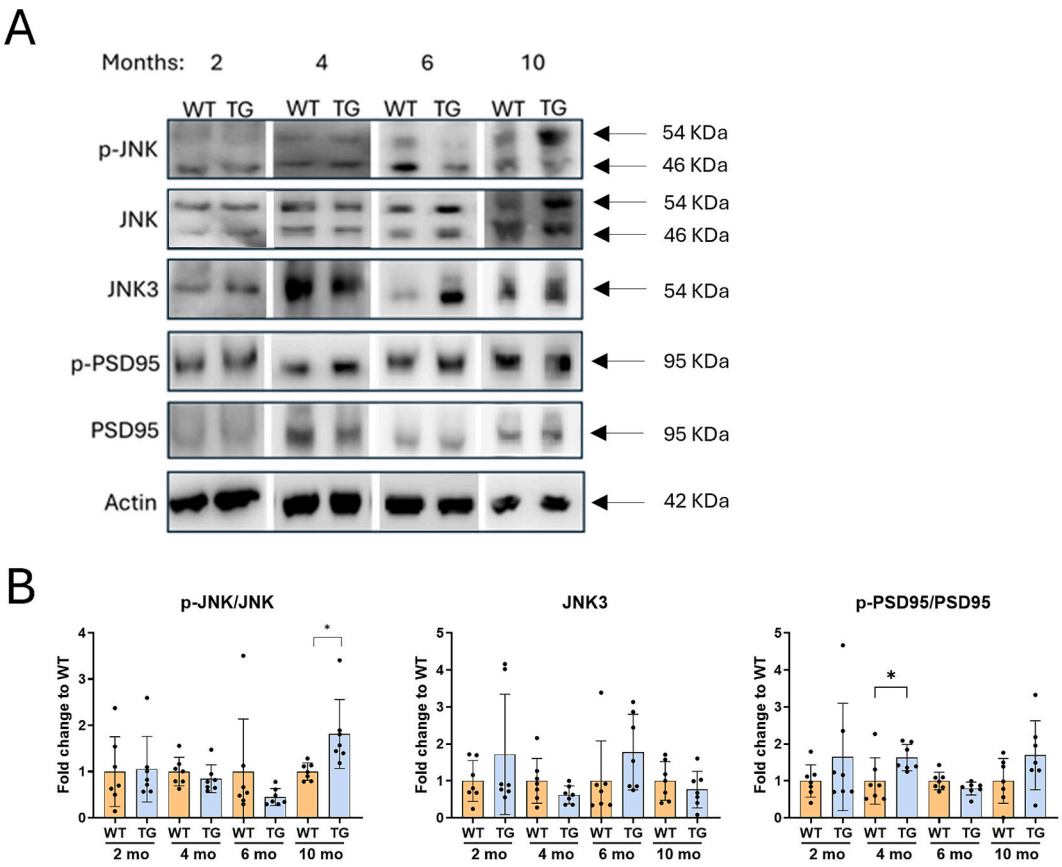


**Fig. 2.** JNK signaling pathway in the retinal postsynaptic-enriched protein fraction. A) Representative cropped images of Western blots of post-synaptic enriched protein fractions of p-JNK, JNK, JNK3, P-PSD95, PSD95, and β-actin (loading control) from WT and 5xFAD B6SJLF1/J (TG) mice at 2, 4, 6, and 10 months of age. B) Quantification of protein levels relative to WT mice, presented as mean ± SD ($n = 7$ per time point). Data are expressed as mean ± SD. Statistical significance is indicated as $^*P < 0.05$.

### *3.3. Absent JNK3 but persistent gliotic GFAP upregulation in 5xFAD mouse retinas*

To evaluate JNK3 and p-JNK expression patterns in 5xFAD B6SJLF1/J retina, we performed immunofluorescence staining (Fig. 3, Fig. S1).

Immunofluorescence revealed nuclear p-JNK expression in the GCL, INL, and outer nuclear layer (ONL) of both WT and 5xFAD B6SJLF1/J mice, with a reduced signal in 5xFAD retinas (Fig. 3, $P = 0.0098$). GFAP staining showed vascular-associated expression in WT mice, while 5xFAD B6SJLF1/J retinas exhibited more intense GFAP staining in Müller cell radial processes, indicative of reactive gliosis without changing global fluorescence intensity in the retina (Fig. 3, Fig. S2). JNK3 expression was minimal in WT retinas at 4 months, whereas 5xFAD B6SJLF1/J mice exhibited enhanced immunofluorescent signal in both the ganglion cell layer (GCL) and inner nuclear layer (INL) (Fig. 3). Quantitative analysis revealed that JNK3 immunoreactivity was overall higher and more uniform in transgenic retinas, while WT samples showed greater heterogeneity across animals. This variability in WT retinas did not obscure the clear increase in JNK3 signal in 5xFAD mice, although further studies with larger cohorts will be needed to determine whether it reflects biological or technical factors.

### *3.4. 5xFAD B6SJLF1/J mice do not exhibit Alzheimer's disease-related marker expression in the retina*

Given the absence of clear JNK pathway activation, we next assessed whether 5xFAD B6SJLF1/J retinas exhibit altered AD marker expression. Digital droplet PCR (ddPCR) detected human amyloid precursor protein (APP) expression exclusively in 5xFAD B6SJLF1/J retinas at 4 months (Fig. 4A, left), while combined human/murine APP levels (normalized to GAPDH) showed no genotype-dependent differences due to predominant murine APP expression (Fig. 4A, right). ELISA analysis revealed comparable amyloid beta 42 (Aβ42) levels between 5xFAD B6SJLF1/J and WT retinal homogenates (Fig. 4B).

Western blot analysis of retinal tissue from 2- to 10-month-old mice confirmed no significant differences in either total APP or phosphorylated APP (p-APP) levels between genotypes (Fig. 4C). This retinal profile contrasts sharply with our previous findings in brain parenchyma, where both APP and p-APP levels increase progressively during disease progression(Priori et al., 2023), indicating fundamental differences in APP metabolism between retinal and brain tissues.

Immunofluorescence analysis of 4-month-old mice confirmed transgenic human APP expression in 5xFAD B6SJLF1/J retinas (Fig. 4D, Fig. S3). While WT retinas showed vascular-associated APP expression in the GCL, 5xFAD B6SJLF1/J retinas exhibited: (1) widespread APP distribution throughout retinal layers, with reduced vascular localization; and (2) decreased p-APP expression compared to WT controls. In WT mice, p-APP was detected in all nuclear layers (GCL, INL, ONL), whereas 5xFAD B6SJLF1/J retinas showed nuclear-restricted p-APP localization primarily in the GCL and INL. Together, these results demonstrate distinct APP handling between retinal and brain tissues in 5xFAD mice, suggesting tissue-specific protection against Alzheimer's-related protein dysregulation.

### *3.5. 5xFAD mice show total retinal thickening with stable INL thickness while WT mice develop INL thinning over time*

Given the increased immunostaining of JNK3 in the GCL and INL and

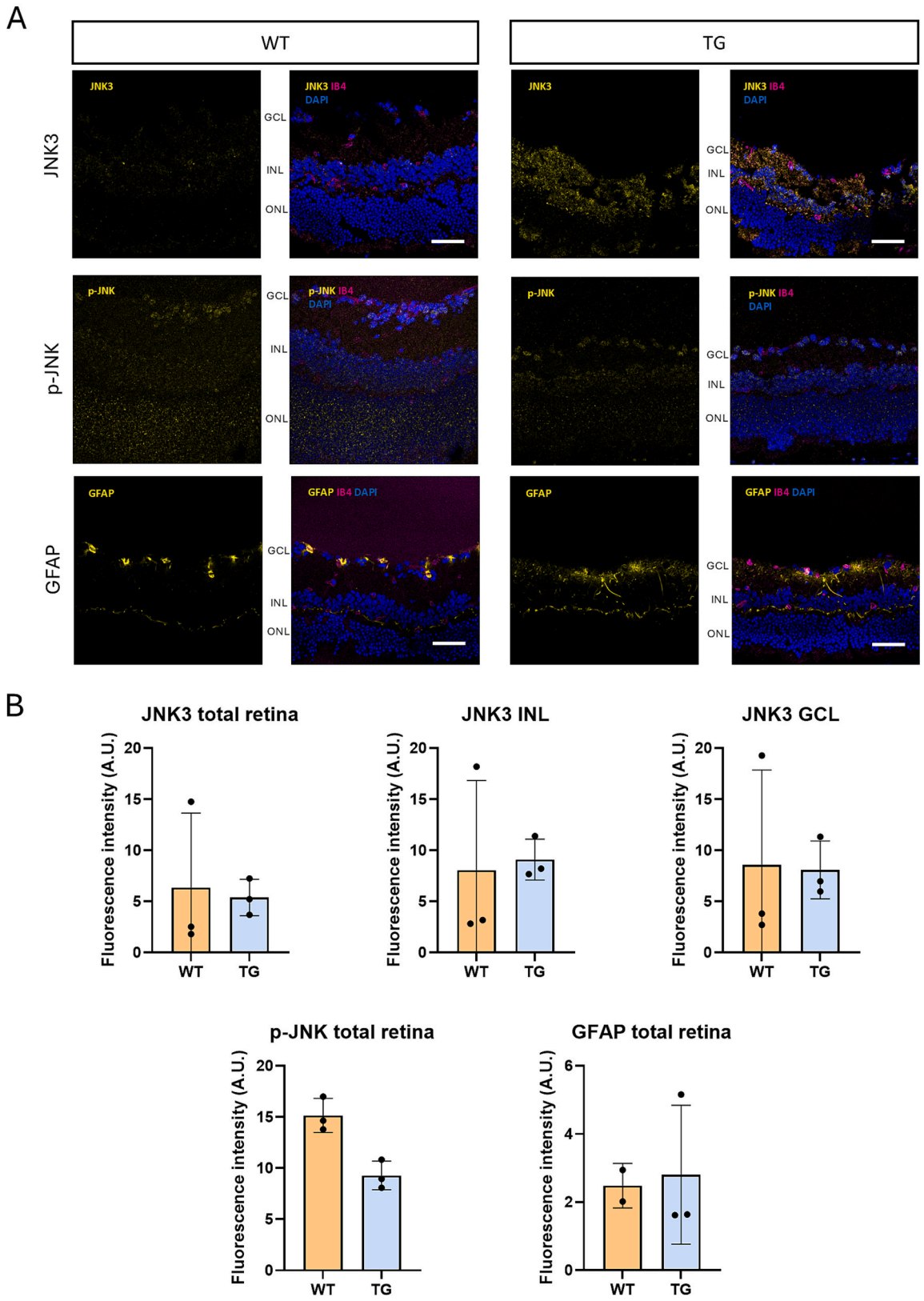


**Fig. 3.** Immunohistochemical analysis of retinal sections in murine samples. A) Representative IHC images of retinal sections of WT and 5xFAD B6SJLF1/J (TG) mice at 4 months of age, showing staining for JNK3, phosphorylated JNK (p-JNK), GFAP, IB4, and DAPI. Scale bars = 50 μm. Images of all mice are presented in Supplemental Fig. 1–2. B) Quantification of total retinal JNK3 immunofluorescence intensity and layer-specific JNK3 immunofluorescence intensity in inner nuclear layer (INL) and the ganglion cell layer (GCL), as well as p-JNK and GFAP fluorescence intensity in total retinal sections from 4-month-old WT and TG mice based on immunofluorescence images ($n = 3$). Data are expressed as mean ± SD.

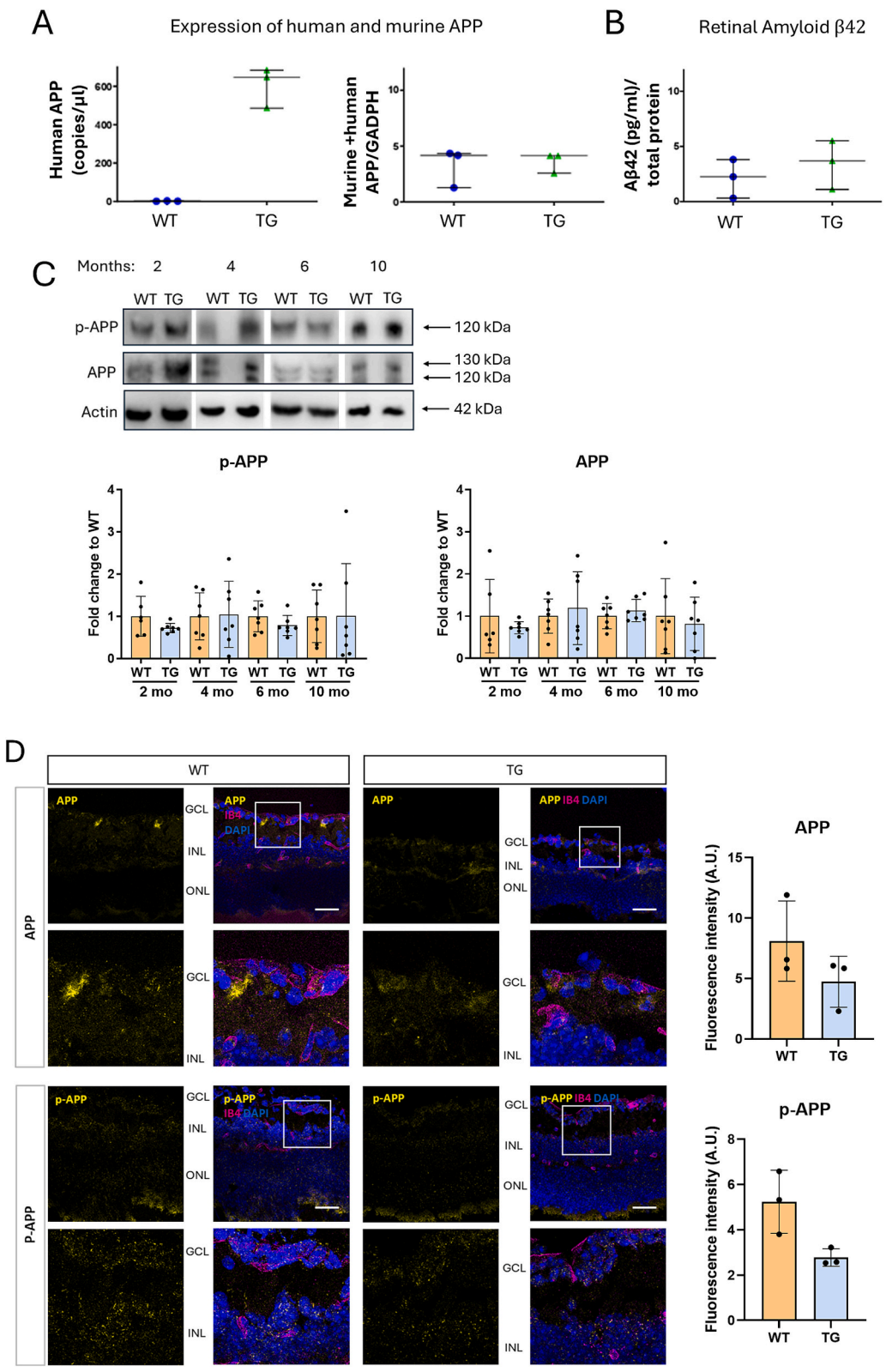


**Fig. 4.** Characterization of amyloid pathology in mouse retina. A) Digital PCR analysis of human and murine APP expression levels in retinal samples of 4-month-old mice ($n = 3$). B) ELISA quantification of Aβ oligomers in retinal tissues from 4-month-old mice (n = 3). C) Representative cropped images of Western blots and quantification of APP and p-APP in 2, 4, 6, 10 months old WT and 5xFAD B6SJLF1/J (TG) mice ($n = 7$ per time point). Data is presented as mean ± SD. D) Representative immunohistochemistry images of retinal sections and magnifications of 4-month-old WT and TG mice showing APP and p-APP localization, co-stained with IB4 and DAPI. Scale bar: 50 µm. Images of all mice are presented in Supplemental Fig. 3. Quantification of the APP and p-APP fluorescence intensity in mouse retina samples from 4-month-old WT and TG mice based on immunofluorescence staining images (n = 3). Data are expressed as mean ± SD.

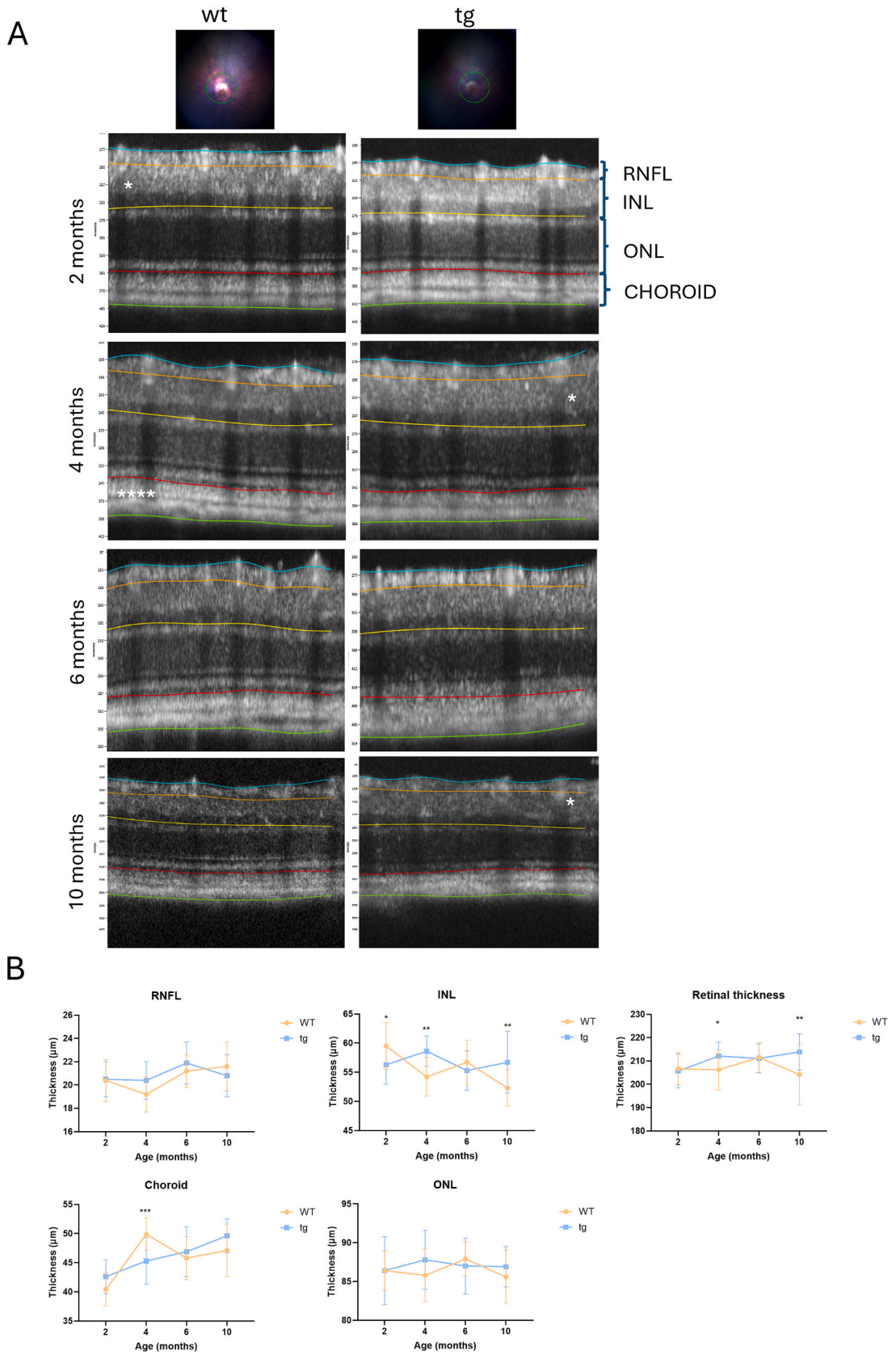


**Fig. 5.** Longitudinal analysis of retinal layer thickness in WT and 5xFAD B6SJLF1/J mice. A) Representative OCT images of the right eye from WT and 5xFAD B6SJLF1/J (TG) mice at 2, 4, 6, and 10 months of age ($n = 7$ per group). The optic nerve head is indicated with a circle.

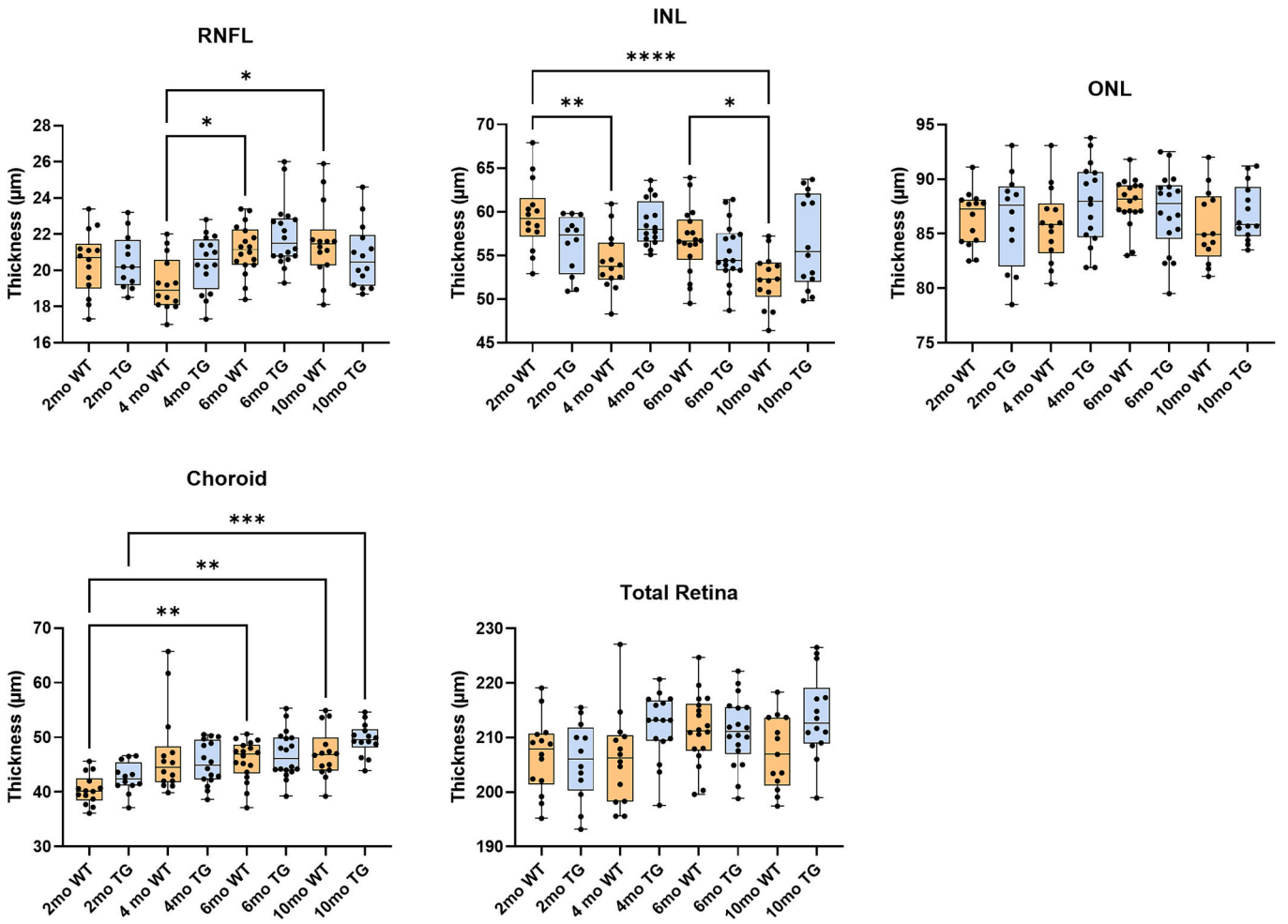


**Fig. 6.** Longitudinal changes in retinal layer thickness. Graphical representation of the longitudinal changes in retinal layer thickness over time for WT and 5xFAD B6SJLF1/J (TG) mice. Statistical analyses were performed using ANOVA. Statistical significance is indicated as *$P < 0.05$, ** $P < 0.01$, *** $P < 0.001$, **** $P < 0.0001$. RNFL, Retinal Nerve Fiber Layer; INL, inner nuclear layer; ONL, outer nuclear layer.

the presence of gliosis in the transgenic mice (Fig. 3), we assessed potential structural changes in retinal layer thickness during the mice 10-month lifespan using OCT (Fig. 5A).

The INL was thinner in 5xFAD B6SJLF1/J at 2 months ($P = 0.028$), but thicker at 4 months ($P = 0.0014$) and 10 months ($P = 0.0019$) (Fig. 5B). The retinal nerve fiber layer (RNFL), existing of axons of ganglion cells, shows a tendency to be thicker in 5xFAD B6SJLF1/J at 4 months ($P = 0.055$), but no differences at other ages. Total retinal thickness was increased in 5xFAD at 4 months ($P = 0.043$) and 10 months ($P = 0.0015$). The choroid was thinner in 5xFAD B6SJLF1/J at 4 months ($P = 0.0007$). No consistent genotype differences were found in ONL.

Longitudinal comparison between 2-month and 10-month time points revealed significant age-related thinning of the INL ($P < 0.0001$) accompanied by choroidal thickening ($P = 0.0022$) in WT mice (Fig. 6). In contrast, TG mice exhibited a tendency to increase in total retinal thickness and similar choroidal thickening ($P < 0.001$), while maintaining stable INL thickness. While both genotypes show choroidal thickening with age, 5xFAD B6SJLF1/J retinas diverge through maintained INL thickness and increased total retinal thickness, indicating genotype-specific differences.

## 4. Discussion

There is increasing evidence that neurodegenerative brain diseases, including AD, often involve retinal pathology, suggesting the retina as a potential "window into the brain" (Simó et al., 2018). This is rooted in their shared embryonic origin and structural similarities, including synaptic networks and vascular systems. Recently, in the context of AD, the concept that detectable changes in the retina may mirror, or diverge, from cerebral pathology has emerged. A key advantage of studying the retina is that these alterations can be assessed through non-invasive imaging, offering a promising pathway for early diagnosis.

Emerging studies also reveal that retinal metabolic dysfunction and oxidative stress closely mirror those in the AD brain (Ravichandran et al., 2024), suggesting overlapping degenerative pathways. To investigate this further, we examined whether retinal neurodegeneration aligns with brain pathology in the previously reported 5xFAD B6SJLF1/J mouse model of AD (Priori et al., 2023) and whether JNK activation is a shared pathogenic mechanism. Retinal changes were tracked across disease progression (2, 4, 6, and 10 months) using OCT imaging, Western blotting and immunofluorescence.

Despite robust cerebral pathology, including amyloid accumulation and JNK activation, the retina of 5xFAD B6SJLF1/J mice showed minimal Aβ oligomer accumulation and no significant APP expression compared to WT mice.

Although amyloid pathology is generally expected to worsen progressively with disease advancement, several studies have shown that in transgenic models such as 5xFAD, amyloid accumulation can reach a plateau at later stages, depending on tissue, region, and genetic background (Javonillo et al., 2021; Liu et al., 2017; Kitazawa et al., 2012; Pádua et al., 2024). In this context, the absence of significant changes

across time points in our retinal analyses may reflect a stabilization of amyloid-related processes rather than a lack of pathology per se, supporting the notion that retinal pathology may evolve independently from cerebral amyloid burden, following a distinct and non-linear trajectory. This corresponded with a lack of JNK pathway activation, as indicated by stable p-JNK/JNK and JNK3 levels in total retinal homogenate as assessed by Western blot.

However, JNK3 is particularly sensitive to changes in the neuronal environment, and immunofluorescence revealed a localized trend toward increased JNK3 signal in 4-month-old 5xFAD B6SJLF1/J mice, especially in the ganglion cell layer (GCL) and inner nuclear layer (INL). Given the observed variability and the limited sample size, these findings should be interpreted as indicative of spatially restricted modulation rather than evidence of a generalized increase in JNK3 immunoreactivity in transgenic mouse retinas. This technique provides superior spatial resolution, allowing detection of compartment-specific alterations that are not evident in whole-retina lysates. Consistently, PSD-enriched fractions showed early increases in PSD95 phosphorylation without changes JNK activation, suggesting that initial postsynaptic dysfunction can arise independently of detectable JNK signaling at the tissue level. Importantly, these changes do not follow a strictly linear temporal progression. Synaptic proteins such as PSD95 are known to exhibit stage-dependent, compensatory, or fluctuating regulation during neurodegenerative disease progression, rather than a monotonic decline (Sultana et al., 2010). Early increases in PSD95 phosphorylation may reflect an adaptive or stress-related postsynaptic response aimed at hyper-stabilizing the postsynaptic density (Dore et al., 2021), a process that precedes overt pathway activation and structural degeneration. Non-linear patterns of synaptic marker regulation, characterized by initial resilience followed by late-stage loss, have been described in both the brain and the retina during AD (Chiquita et al., 2019; Bevan et al., 2020). Similarly, in 5xFAD mice, structural and synaptic retinal alterations appear at early disease stages without following a strict age-dependent progression (Lim et al., 2020; Zhang et al., 2021), supporting the interpretation that PSD95 phosphorylation changes reflect dynamic synaptic remodelling rather than a monotonic temporal trend, highlighting the complexity of synaptic remodelling during disease evolution. These localized changes likely precede broader pathway activation and may relate to early JNK3 engagement at the synapse. Elevated GFAP in Müller cells further indicated early gliosis and neuroinflammation, reinforcing that localized retinal pathology can occur in the absence of overt global biochemical changes. By 10 months, increased p-JNK/JNK ratios in TIF fractions indicated later-stage, more widespread activation of JNK isoforms, making these changes detectable by Western blot. This temporal progression supports a model in which early, spatially restricted signaling events eventually converge into broader stress pathway activation. Together, these findings emphasize that subcellular and cell-type–specific analyses are essential for detecting early retinal alterations in this model and illustrate how localized molecular changes may precede or even diverge from global pathological readouts.

Strikingly, no retinal Aβ aggregation was detected, strongly contrasting with the Aβ42 accumulation in the brain (Priori et al., 2023), aligning with some human studies (den Haan et al., 2018). However, our findings must be interpreted within the context of a complex and sometimes contradictory body of literature on retinal pathology in 5xFAD mice. A key factor underlying these inconsistencies is the influence of genetic background. Although all 5xFAD colonies carry the same transgenes, their backgrounds can markedly modulate Aβ kinetics, inflammatory tone, and neuronal vulnerability. The B6SJLF1/J hybrid background combines C57BL/6J and SJL/J contributions, introducing genetic diversity that better reflects the heterogeneity observed in human populations and potentially broadens the translational relevance of the model. However, this diversity also alters disease expression. Mouse background can influence the timing and extent of amyloid accumulation, retinal thickening, and synaptic alterations, as shown by differences among B6SJLF1/J, C57BL/6J, and SJL/J 5xFAD lines. For instance, (Nam et al., 2022) reported delayed Aβ deposition in SJL/J 5xFAD mice, while early Aβ42 accumulation was observed in C57BL/6J strains (Matei et al., 2022 Nam et al., 2022; Parthasarathy et al., 2015). These discrepancies suggest that the hybrid background may attenuate or delay retinal involvement, even when central pathology is pronounced. Thus, although the B6SJLF1/J background provides valuable genetic heterogeneity, it also highlights important limitations when attempting to model the full spectrum of AD-related retinal changes and underscores the need to consider background-dependent variability when comparing findings across studies. Detection methods should also be taken into account. Using alternative antibodies, (Jovanovic Macura et al., 2023) detected Aβ in 5xFAD B6SJLF1/J mice at 4 and 12 months, emphasizing the methodological sensitivity required to detect subtle retinal pathology (Jovanovic Macura et al., 2023). In addition, antibody selection, tissue preparation, imaging resolution, and sample processing can markedly affect the detection of subtle pathological features, including Aβ aggregation and JNK activation. These considerations likely explain why some studies report early retinal amyloid deposits, whereas our data highlight selective synaptic alterations without robust Aβ accumulation. A further limitation of the present study is the relatively small sample size, particularly with respect to sex-based comparisons, which precludes definitive conclusions regarding sex-dependent effects. The small sample size limits the statistical power to detect differences in immunofluorescence intensity, requiring cautious interpretation of JNK3 and GFAP upregulation. Moreover, variability within the WT groups likely arises from both biological heterogeneity in retinal structure and technical factors related to OCT acquisition and segmentation, emphasizing the need for larger, well-powered studies to validate quantitative retinal findings.

OCT in our mouse model shows similarities with the findings reported by Lynn et al. (Lynn et al., 2025). We described an increase in the INL layer thickness in 5xFAD mice at 10 months that may be due to thickening of photoreceptor nuclei and inner segments in 5xFAD retinas; as reported by Lynn et al. at 8 months of age. Moreover; their study of chorioretinal tissues revealed diminished photoreceptor nuclei in 4-month-old 5xFAD eyes; and we observed a reduction of the choroid layer thickness by OCT in our 5xFAD mouse model. However; unexpectedly; our longitudinal OCT data revealed retinal thickening over time; rather than the expected thinning; potentially reflecting Müller cell swelling and gliotic remodelling. Similar findings have been reported (Zhang et al., 2021); although others observed retinal thinning (Kim et al., 2021) or no changes (Matei et al., 2022; McCool et al., 2025); further underscoring the influence of strain background and temporal progression (Creighton et al., 2019; Lim et al., 2020). Recently; Ladurner et al.; (Ladurner et al., 2025) reached similar conclusions by performing retinal OCT investigations in three mouse models of Alzheimer's disease. The authors reported that retinal parameters were unique to each AD mouse model, indicating fundamental phenotypic differences.

In line with our findings, Zhang et al. (2021) also reported early structural retinal changes in 5xFAD mice before the onset of robust functional deficits. They observed thickening of the outer nuclear layer (ONL) at 4 months; followed by general retinal thickening at 6 months; accompanied by glial activation and a modest increase in amyloid plaques. Importantly; they documented that this structural remodelling preceded major functional decline: at 6 months the mice showed impaired visual behaviour (optomotor test) and reduced light responses of retinal ganglion cells (via multielectrode-array); while full-field ERG and pERG remained relatively preserved. These observations parallel our OCT-based detection of retinal thickening at early ages and support the hypothesis that structural changes; rather than synapse loss or massive amyloid deposition; may be among the first detectable retinal pathologies in 5xFAD. On the other hand; while Zhang et al. reported more amyloid plaques (albeit few) in the retina by 6 months; our study found no robust Aβ aggregation at similar or earlier timepoints; suggesting a divergence in the timeline or magnitude of amyloid

accumulation(Zhang et al., 2021).

In summary, our study highlights a compartmentalized and non-linear relationship between retinal and cerebral pathology in the 5xFAD model of Alzheimer's disease. While the 5xFAD B6SJLF1/J model faithfully recapitulates cerebral AD phenotypes, including Aβ deposition and JNK activation (Priori et al., 2023), the retina may follow a distinct trajectory. This is possibly driven by alternative stress pathways or compensatory remodelling and is characterized by early synaptic dysfunction, spatially restricted alterations in JNK3 immunoreactivity and gliosis, and paradoxical thickening, all occurring without extensive Aβ deposition or global JNK activation.

However, based on the present dataset, we refrain from concluding that JNK3 is globally increased in transgenic retinas and instead propose that early changes are spatially restricted and require validations in larger cohorts. Differences in APP expression and Aβ processing between brain and retina, shaped by regional regulation and strain background, may underlie these divergent outcomes.

Importantly, our results reconcile prior conflicting reports by demonstrating that subtle retinal alterations may precede overt amyloid pathology and functional deficits, supporting the retina as a sensitive but independent window into neurodegeneration.

These findings support the retina's potential as a sensitive site for monitoring neurodegenerative changes but also emphasize the importance of methodological rigor and strain consideration. The retina does reflect brain pathology, but not as a simple mirror. It may offer an early glimpse into neurodegeneration, albeit through its own molecular lens.

## CRediT authorship contribution statement

**A. Giani:** Writing – review & editing, Writing – original draft, Methodology, Investigation, Formal analysis. **C.A. Musi:** Writing – review & editing, Writing – original draft, Methodology, Investigation, Formal analysis, Data curation. **E.C. Priori:** Writing – review & editing, Writing – original draft, Methodology, Investigation, Formal analysis, Data curation. **S. Turchetti:** Writing – review & editing, Formal analysis. **M. Passi:** Writing – review & editing, Writing – original draft, Methodology, Formal analysis. **S. Galbiati:** Writing – review & editing, Writing – original draft, Methodology, Investigation, Formal analysis, Data curation. **I. Viganò:** Writing – review & editing, Methodology, Investigation, Formal analysis. **N. Bakker:** Writing – review & editing, Writing – original draft, Methodology, Investigation, Formal analysis. **I. Klaassen:** Writing – review & editing, Writing – original draft, Supervision, Funding acquisition, Formal analysis, Conceptualization. **G. Zerbini:** Writing – review & editing, Supervision, Investigation, Funding acquisition, Conceptualization. **T. Borsello:** Writing – review & editing, Supervision, Project administration, Funding acquisition, Conceptualization.

## Funding

This study was funded by the European Commission (H2020 programme-GA 847749).

## Declaration of competing interest

All authors have seen and approved the final version of the manuscript, and no conflicts of interest are declared.

## Appendix A. Supplementary data

Supplementary data to this article can be found online at https://doi.org/10.1016/j.expneurol.2026.115758.

## Data availability

The datasets generated during and/or analyzed during the current study are available from the corresponding author upon reasonable request.

## References

Alexandrov, Peter N., Pogue, Aileen, Bhattacharjee, Surjyadipta, Lukiw, Walter J., 2011. Retinal amyloid peptides and complement factor h in transgenic models of alzheimers disease. Neuroreport 22 (12), 623–627. https://doi.org/10.1097/WNR.0b013e3283497334.

Bevan, Ryan J., Hughes, Tim R., Williams, Pete A., Good, Mark A., Paul Morgan, B., Morgan, James E., 2020. Retinal ganglion cell degeneration correlates with hippocampal spine loss in experimental alzheimers disease. Acta Neuropathol. Commun. 8 (1), 216. https://doi.org/10.1186/s40478-020-01094-2.

Biessels, G.J., De Leeuw, F.E., Lindeboom, J., Barkhof, F., Scheltens, P., 2006. Increased cortical atrophy in patients with alzheimers disease and type 2 diabetes mellitus. J. Neurol. Neurosurg. Psychiatry 77 (3), 304–307. https://doi.org/10.1136/jnnp.2005.069583.

Biggi, Silvia, Buccarello, Lucia, Sclip, Alessandra, et al., 2017. Evidence of presynaptic localization and function of the C-Jun N-terminal kinase. Neural Plast. 2017, 6468356. https://doi.org/10.1155/2017/6468356.

Buccarello, Lucia, Sclip, Alessandra, Sacchi, Matteo, et al., 2017. The C-Jun N-terminal kinase plays a key role in ocular degenerative changes in a mouse model of alzheimer disease suggesting a correlation between ocular and brain pathologies. Oncotarget 8 (47), 83038–83051. https://doi.org/10.18632/oncotarget.19886.

Chiquita, Samuel, Campos, Elisa J., Castelhano, João, et al., 2019. Retinal thinning of inner sub-layers is associated with cortical atrophy in a mouse model of alzheimers disease: a longitudinal multimodal in vivo study. Alzheimer's Res. Ther. 11 (1), 90. https://doi.org/10.1186/s13195-019-0542-8.

Coffey, Eleanor T., 2014. Nuclear and cytosolic JNK signalling in neurons. Nat. Rev. Neurosci. 15 (5), 285–299. https://doi.org/10.1038/nrn3729.

Creighton, S.D., Mendell, A.L., Palmer, D., et al., 2019. Dissociable cognitive impairments in two strains of transgenic Alzheimer's disease mice revealed by a battery of object-based tests. Sci. Rep. 9 (1), 57. https://doi.org/10.1038/s41598-018-37312-0.

den Haan, J., Morrema, T.H.J., Verbraak, F.D., et al., 2018. Amyloid-beta and phosphorylated tau in post-mortem Alzheimer's disease retinas. Acta Neuropathol. Commun. 6 (1), 147. https://doi.org/10.1186/s40478-018-0650-x.

Dore, K., Carrico, Z., Alfonso, S., et al., 2021. PSD-95 protects synapses from β-amyloid. Cell Rep 35 (9), 109194. https://doi.org/10.1016/j.celrep.2021.109194.

Doustar, Jonah, Torbati, Tania, Black, Keith L., Koronyo, Yosef, Koronyo-Hamaoui, Maya, 2017. Optical coherence tomography in alzheimers disease and other neurodegenerative diseases. Front. Neurol. 8, 701. https://doi.org/10.3389/fneur.2017.00701.

Du, Hongjun, Sun, Xufang, Guma, Monica, et al., 2013. JNK inhibition reduces apoptosis and neovascularization in a murine model of age-related macular degeneration. Proc. Natl. Acad. Sci. USA 110 (6), 2377–2382. https://doi.org/10.1073/pnas.1221729110.

Dutescu, R. Michael, Li, Qiao-Xin, Crowston, Jonathan, Masters, Colin L., Baird, Paul N., Culvenor, Janetta G., 2009. Amyloid precursor protein processing and retinal pathology in mouse models of alzheimers disease. Graefes Arch. Clin. Exp. Ophthalmol. 247 (9), 1213–1221. https://doi.org/10.1007/s00417-009-1060-3.

Gaire, Bhakta Prasad, Koronyo, Yosef, Fuchs, Dieu-Trang, et al., 2024. Alzheimers disease pathophysiology in the retina. Prog. Retin. Eye Res. 101 (July), 101273. https://doi.org/10.1016/j.preteyeres.2024.101273.

Galy, Anne, Roux, Michel Joseph, Sahel, José Alain, Léveillard, Thierry, Giangrande, Angela, 2005. Rhodopsin maturation defects induce photoreceptor death by apoptosis: a fly model for RhodopsinPro23His human retinitis pigmentosa. Hum. Mol. Genet. 14 (17), 2547–2557. https://doi.org/10.1093/hmg/ddi258.

Gardoni, F., Schrama, L.H., Kamal, A., Gispen, W.H., Cattabeni, F., Di Luca, M., 2001a. Hippocampal synaptic plasticity involves competition between Ca2+/calmodulin-dependent protein kinase II and postsynaptic density 95 for binding to the NR2A subunit of the NMDA receptor. J. Neurosci. 21 (5), 1501–1509.

Gardoni, F., Schrama, L.H., Kamal, A., Gispen, W.H., Cattabeni, F., Di Luca, M., 2001b. Hippocampal synaptic plasticity involves competition between Ca2+/calmodulin-dependent protein kinase II and postsynaptic density 95 for binding to the NR2A subunit of the NMDA receptor. J. Neurosci. 21 (5), 1501–1509. https://doi.org/10.1523/JNEUROSCI.21-05-01501.2001.

Gardoni, Fabrizio, Sgobio, Carmelo, Pendolino, Valentina, Calabresi, Paolo, Di Luca, Monica, Picconi, Barbara, 2012. Targeting NR2A-containing NMDA receptors reduces L-DOPA-induced dyskinesias. Neurobiol. Aging 33 (9), 2138–2144. https://doi.org/10.1016/j.neurobiolaging.2011.06.019.

Guma, Monica, Rius, Jordi, Duong-Polk, Karen X., Haddad, Gabriel G., Lindsey, James D., Karin, Michael, 2009. Genetic and pharmacological inhibition of JNK ameliorates hypoxia-induced retinopathy through interference with VEGF expression. Proc. Natl. Acad. Sci. USA 106 (21), 8760–8765. https://doi.org/10.1073/pnas.0902659106.

Hinton, D.R., Sadun, A.A., Blanks, J.C., Miller, C.A., 1986. Optic-nerve degeneration in alzheimers disease. N. Engl. J. Med. 315 (8), 485–487. https://doi.org/10.1056/NEJM198608213150804.

Javonillo, Dominic I., Tran, Kristine M., Phan, Jimmy, et al., 2021. Systematic phenotyping and characterization of the 3xTg-AD mouse model of alzheimers disease. Front. Neurosci. 15, 785276. https://doi.org/10.3389/fnins.2021.785276.

Jin, Zi, Wang, Xinmin, Lang, Ying, et al., 2025. Retinal optical coherence tomography intensity spatial correlation features as new biomarkers for confirmed alzheimers disease. Alzheimer's Res. Ther. 17 (1), 33. https://doi.org/10.1186/s13195-025-01676-z.

Jovanovic Macura, I., Zivanovic, A., Perovic, M., et al., 2023. The Expression of major facilitator superfamily domain-containing protein2a (Mfsd2a) and aquaporin 4 is altered in the retinas of a 5xFAD mouse model of Alzheimer's disease. Int. J. Mol. Sci. 24 (18), 14092. https://doi.org/10.3390/ijms241814092.

Kang, Min-Ji, Chung, Jaehoon, Ryoo, Hyung Don, 2012. CDK5 and MEKK1 mediate pro-apoptotic signalling following endoplasmic reticulum stress in an autosomal dominant retinitis pigmentosa model. Nat. Cell Biol. 14 (4), 409–415. https://doi.org/10.1038/ncb2447.

Kim, T.H., Son, T., Klatt, D., Yao, X., 2021. Concurrent OCT and OCT angiography of retinal neurovascular degeneration in the 5XFAD Alzheimer's disease mice. Neurophotonics 8 (3), 035002. https://doi.org/10.1117/1.NPh.8.3.035002.

Kitazawa, Masashi, Medeiros, Rodrigo, Laferla, Frank M., 2012. Transgenic mouse models of alzheimer disease: developing a better model as a tool for therapeutic interventions. Curr. Pharm. Des. 18 (8), 1131–1147. https://doi.org/10.2174/138161212799315786.

Kopf, Daniel, Frölich, Lutz, 2009. Risk of incident alzheimers disease in diabetic patients: a systematic review of prospective trials. J. Alzheimer's Dis. JAD 16 (4), 677–685. https://doi.org/10.3233/JAD-2009-1011.

Ladurner, Georg, Harper, Danielle J., May, Lucas, et al., 2025. Comparative investigation of the retinal phenotype of three mouse models of alzheimers disease with optical coherence tomography. Invest. Ophthalmol. Vis. Sci. 66 (14), 35. https://doi.org/10.1167/iovs.66.14.35.

Lim, Jeremiah K.H., Li, Qiao-Xin, He, Zheng, et al., 2020. Retinal functional and structural changes in the 5xFAD mouse model of alzheimers disease. Front. Neurosci. 14, 862. https://doi.org/10.3389/fnins.2020.00862.

Liu, Peng, Reichl, John H., Rao, Eshaan R., et al., 2017. Quantitative comparison of dense-Core amyloid plaque accumulation in amyloid-β protein precursor transgenic mice. J. Alzheimer's Dis. JAD 56 (2), 743–761. https://doi.org/10.3233/JAD-161027.

Lynn, Savannah A., Pandi, Sudha Priya Soundara, Sanchez-Bretano, Aida, et al., 2025. A longitudinal study of the 5xFAD mouse retina delineates amyloid beta (aβ)-mediated retinal pathology from age-related changes. Alzheimer's Res. Ther. 17 (1), 136. https://doi.org/10.1186/s13195-025-01784-w.

Matei, N., Leahy, S., Blair, N.P., et al., 2022. Retinal vascular physiology biomarkers in a 5XFAD mouse model of Alzheimer's disease. Cells 11 (15), 2413. https://doi.org/10.3390/cells11152413.

McCool, S., Smith, J.C., Sladek, A., et al., 2025. Retinal and thalamic alterations in the 5xFAD mouse model of Alzheimer's disease. PLoS One 20 (3), e0319397. https://doi.org/10.1371/journal.pone.0319397.

Musi, Clara Alice, Agrò, Graziella, Buccarello, Lucia, Camuso, Serena, Borsello, Tiziana, 2020. JNK signaling activation in the ube3a maternal deficient mouse model: its specific inhibition prevents post-synaptic protein-enriched fraction alterations and cognitive deficits in angelman syndrome model. Neurobiol. Dis. 140 (July), 104812. https://doi.org/10.1016/j.nbd.2020.104812.

Musi, Clara Alice, Marchini, Giacomo, Giani, Arianna, et al., 2022. Colocalization and interaction study of neuronal JNK3, JIP1, and β-Arrestin2 together with PSD95. Int. J. Mol. Sci. 23 (8), 4113. https://doi.org/10.3390/ijms23084113.

Nam, Y., Kim, S., Kim, J., Hoe, H.S., et al., 2022. Mesoscopic mapping of visual pathway in a female 5XFAD mouse model of Alzheimer's disease. Cells 11 (23), 3901. https://doi.org/10.3390/cells11233901.

Ordoñez, Olivares, Antonio, Marco, Smith, Rebekah Cossette, Yiu, Glenn, Liu, Yin Allison, 2025. Retinal microstructural and microvascular changes in alzheimer disease: a review. Int. Ophthalmol. Clin. 65 (1), 59–67. https://doi.org/10.1097/IIO.0000000000000549.

Pádua, Mafalda Soares, Guil-Guerrero, José L., Prates, José A.M., Lopes, Paula Alexandra, 2024. Insights on the use of transgenic mice models in alzheimers disease research. Int. J. Mol. Sci. 25 (5), 2805. https://doi.org/10.3390/ijms25052805.

Parisi, V., Restuccia, R., Fattapposta, F., Mina, C., Bucci, M.G., Pierelli, F., 2001. Morphological and functional retinal impairment in alzheimers disease patients. Clin. Neurophysiol. 112 (10), 1860–1867. https://doi.org/10.1016/s1388-2457(01)00620-4.

Parthasarathy, R., Chow, K.M., Derafshi, Z., et al., 2015. Reduction of amyloid-beta levels in mouse eye tissues by intra-vitreally delivered neprilysin. Exp. Eye Res. 138, 134–144. https://doi.org/10.1016/j.exer.2015.06.027.

Ploia, Cristina, Antoniou, Xanthi, Sclip, Alessandra, et al., 2011. JNK plays a key role in tau hyperphosphorylation in alzheimers disease models. J. Alzheimer's Dis. JAD 26 (2), 315–329. https://doi.org/10.3233/JAD-2011-110320.

Priori, Erica Cecilia, Musi, Clara Alice, Giani, Arianna, et al., 2023. JNK activation correlates with cognitive impairment and alteration of the post-synaptic element in the 5xFAD AD mouse model. Cells 12 (6), 904. https://doi.org/10.3390/cells12060904.

Ravichandran, S., Snyder, P.J., Alber, J., et al., 2024. Quantifying putative retinal gliosis in preclinical alzheimer's disease. Invest. Ophthalmol. Vis. Sci. 65 (5), 5. https://doi.org/10.1167/iovs.65.5.5.

Safiri, Saeid, Ghaffari Jolfayi, Amir, Fazlollahi, Asra, et al., 2024. Alzheimers disease: a comprehensive review of epidemiology, risk factors, symptoms diagnosis, management, caregiving, advanced treatments and associated challenges. Front. Med. 11 (December). https://doi.org/10.3389/fmed.2024.1474043.

Salobrar-Garcia, Elena, Méndez-Hernández, Carmen, de Hoz, Rosa, et al., 2020. Ocular vascular changes in mild alzheimers disease patients: foveal avascular zone, choroidal thickness, and ONH hemoglobin analysis. J. Personal. Med. 10 (4), 231. https://doi.org/10.3390/jpm10040231.

Sclip, Alessandra, Antoniou, Xanthi, Colombo, Alessio, et al., 2011. C-Jun N-terminal kinase regulates soluble aβ oligomers and cognitive impairment in AD mouse model. J. Biol. Chem. 286 (51), 43871–43880. https://doi.org/10.1074/jbc.M111.297515.

Sclip, Alessandra, Arnaboldi, Andrea, Colombo, Isabella, et al., 2013. Soluble aβ oligomer-induced synaptopathy: C-Jun N-terminal kinases role. J. Mol. Cell Biol. 5 (4), 277–279. https://doi.org/10.1093/jmcb/mjt015.

Sclip, A., Tozzi, A., Abaza, A., et al., 2014. C-Jun N-terminal kinase has a key role in alzheimer disease synaptic dysfunction in vivo. Cell Death Dis. 5 (January), e1019. https://doi.org/10.1038/cddis.2013.559.

Simó, Stitt, A.W., Gardner, T.W., 2018 Sep. Neurodegeneration in diabetic retinopathy: does it really matter? Diabetologia 61 (9), 1902–1912. https://doi.org/10.1007/s00125-018-4692-1.

Sultana, R., Banks, W.A., Butterfield, D.A., 2010. Decreased levels of PSD95 and two associated proteins and increased levels of BCl2 and caspase 3 in hippocampus from subjects with amnestic mild cognitive impairment: Iinsights into their potential roles for loss of synapses and memory, accumulation of Abeta, and neurodegeneration in a prodromal stage of Alzheimer's disease. J. Neurosci. Res. 88 (3), 469–477. https://doi.org/10.1002/jnr.22227.

Vandenabeele, Marjan, Veys, Lien, Lemmens, Sophie, et al., 2021. The AppNL-G-F mouse retina is a site for preclinical alzheimers disease diagnosis and research. Acta Neuropathol. Commun. 9 (1), 6. https://doi.org/10.1186/s40478-020-01102-5.

Zhang, Mengrong, Zhong, Liting, Han, Xiu, et al., 2021. Brain and retinal abnormalities in the 5xFAD mouse model of alzheimers disease at early stages. Front. Neurosci. 15 (July). https://doi.org/10.3389/fnins.2021.681831.

Zhou, Xiaokun, Yi, Wenxiang, Zhi, Yiqiang, et al., 2023. Stress-activated protein kinase JNK modulates depression-like behaviors in mice. Mol. Neurobiol. 60 (5), 2367–2378. https://doi.org/10.1007/s12035-023-03209-x.

Zerbini, G., Maestroni, S., Viganò, I., et al., 2023. Progressive thinning of retinal nerve fiber layer/ganglion cell layer (RNFL/GCL) as biomarker and pharmacological target of diabetic retinopathy. Int. J. Mol. Sci. 24 (16), 12672. https://doi.org/10.3390/ijms241612672.